Meteorol. Z. (Contrib. Atm. Sci.), PrePub DOI 10.1127/metz/2020/1012

PrePub Article

On ice supersaturation over the Arctic

Klaus Gierens[1*], Lena Wilhelm[2], Michael Sommer[3] and Dan Weaver[4]

[1]Deutsches Zentrum für Luft- und Raumfahrt (DLR) – Institut für Physik der Atmosphäre, Oberpfaffenhofen, Germany
[2]Universität Bonn, now at Universität Hohenheim, Germany
[3]GRUAN Lead Centre, Meteorologisches Observatorium Lindenberg, Germany
[4]Dept. of Physical and Environmental Sciences, University of Toronto Scarborough, Toronto, Canada

(Manuscript received December 5, 2019; in revised form February 19, 2020; accepted February 21, 2020)

Abstract

We study ice-supersaturation in the cold (< −38°C) arctic troposphere and lower stratosphere using high-resolution quality-controlled radiosonde data. On average, ice supersaturation occurs in about 40 % to 60 % of the profiles with frequency of occurrence increasing with geographic latitude. The frequencies of occurrence show (so far) no long-term trends. The seasonal cycles are not very clear but seem to reverse between more southern to more northern locations. Most profiles with ice-supersaturation have more than one supersaturated layer; this stacking increases as well to the north. Due to the 1-Hz resolution of the data we find ice-supersaturated layers a few metres thick, but very thick layers extending over almost 5 km are found as well. Median thickness values are smaller than in previous studies, between 100 m and 200 m. The far northern locations display a strong seasonal cycle of the mean layer thickness with maxima in the polar night, probably caused by radiation cooling. Ice supersaturation occurs most frequently directly beneath the tropopause in an upper-tropospheric layer whose depth varies strongly seasonally, being thin in summer and much thicker in winter. Due to the very low temperatures in the Arctic ice supersaturation can occur at the ground. Temperatures in arctic supersaturated layers typically range from −40 to −60 °C, but can occasionally be lower than −70 °C. Water vapour volume mixing ratios range from a few to about 500 ppmv. The relative humidity with respect to ice can exceed 150–160 %. The thickness of supersaturated layers is weakly correlated with its maximum supersaturation, but not with temperature and absolute humidity.

Keywords: ice supersaturation, Arctic, radiosonde data, GRUAN

1 Introduction

The Arctic is a region where climate change is particularly strong, with near-surface temperatures increasing almost twice as fast than elsewhere (Hassol, 2004). The temperature increase is stronger in winter than on annual average and stronger over the ocean than over land. Another wellknown effect is the reduction of arctic sea ice; both its horizontal extent as well as its volume shrink leaving larger and larger areas of open water, i.e. a huge source for water vapour. This implies that higher temperatures, leading to higher water vapour saturation pressures, will be followed by higher amounts of water vapour in (at least) the troposphere when we assume that the average relative humidity (RH) will not change substantially. However, general circulation models show a quite robust pattern of RH changes in a warmer climate with an increase of RH in the arctic upper troposphere and lower stratosphere (Sherwood et al., 2010; Wright et al., 2010; Irvine and Shine, 2015). Thus, phenomena related to relative humidity like cirrus cloudiness and its precondition, ice supersaturation, may be expected to increase as well in future. As these and more changes have consequences for the whole world (e.g. sea level rise), monitoring the arctic is necessary by all sorts of instruments (e.g. Weaver et al., 2017; Alraddawi et al., 2018; Scarlat et al., 2018; Mech et al., 2019; Weaver et al., 2019), in order to understand the origin of the changes, their magnitude and their eventual impacts on the local and global society.

The present paper focusses on the phenomenon of ice supersaturation in the arctic atmosphere. As such it stands in a distinguished tradition, since the first measurement of ice supersaturation in the atmosphere was made 1906 by Alfred Wegener on Greenland (Wegener, 1914; Gierens et al., 2012). In spite of this early measurement, not much is known about ice supersaturation in the arctic and it is currently hardly possible to detect any decadal changes, simply because the data basis for that purpose is too sparse. Ice supersaturation is a special but frequent state of the humidity field, where the relative humidity with respect to ice, RH_i, exceeds 100 %. It seems to occur quite often in arctic latitudes (e.g. Gierens et al., 2004). It is prerequisite for cirrus formation (Heymsfield et al., 1998) and indeed often (if not mostly) found within cirrus clouds (Ovarlez et al., 2002; Spichtinger et al., 2004; Krämer et al., 2016) but also in clear sky since formation of cirrus by homogeneous nucleation needs high ice supersaturation

*Corresponding author: Klaus Gierens, DLR Oberpfaffenhofen, Institut für Physik der Atmosphäre, Oberpfaffenhofen, 82234 Wessling, Germany, e-mail: klaus.gierens@dlr.de

(Koop et al., 2000). As the relative humidity is expected to increase in the arctic UTLS (upper troposphere and lower stratosphere), it is conceivable that ice supersaturation will occur more frequently. However, subsequent cirrus formation followed by sedimentation of ice crystals and thus removal of excess water will limit the increase of ice supersaturation.

Of course there are influences on water vapour and ice supersaturation on shorter time scales as well and it is necessary to understand them. The data source with best coverage of the arctic atmosphere is satellites, in particular limb-sounding instruments. Unfortunately, these instruments do not always provide regular and uniform sampling, and this can cause biases when the observed field (here the humidity field) has strong gradients and temporal variability. Water vapour variability is large in the upper troposphere and thus quite substantial biases must be taken into account when corresponding studying satellite data. Sioris et al. (2016) studied the influence of annular modes, that is, the north atlantic and arctic oscillation (Thompson and Wallace, 2000), on the budget of water vapour in the arctic upper troposphere and lowermost stratosphere using satellite-borne limb-profilers (solar occultation instruments) that combine high vertical resolution with the ability to probe water vapour throughout the free troposphere and up into the very dry regions above the tropopause where the volume mixing ratio (WVMR) falls below 10 ppmv. They report a strong seasonal variation of WVMR in the arctic upper troposphere that follows approximately the seasonal cycle of the saturation mixing ratio; in contrast the lower stratosphere exhibits a weak seasonal cycle that is disconnected to the cycle of the saturation value, a signature of the lacking large source of water vapour in this altitude region. The response of WVMR anomalies to the phase of the arctic oscillation is strong in the upper troposphere, but decreasing with altitude and vanishing at the tropopause.

Kempter (2016) selected special cases from data on upper-tropospheric humidity provided by the High-resolution Infrared Sounder (HIRS) on the National Oceanic and Atmospheric Agency (NOAA) polar orbiting satellites NOAA 14 and NOAA 15. These were cases where the retrieval method of Jackson and Bates (2001) indicated ice supersaturation. The central result of this selection was that such cases appear only in winter and only north of 55°. Of course, ice supersaturation exists at lower latitudes as well but it is difficult to detect the relatively thin (Spichtinger et al., 2003b; Dickson et al., 2010a) ice supersaturated layers in coarse-resolution data from nadir sounders (see Gierens et al., 2004). Thus the most economic interpretation of Kempter's finding was that there must be very thick ice supersaturated regions in the Arctic in winter and the thickness of these regions might be explained by constant radiation cooling in the dark season. Such an explanation has also been given for the very extended ice supersaturated regions that occur in the Antarctic winter (Spichtinger et al., 2003a).

In the present paper we study arctic ice supersaturated regions (ISSRs), determine some of their properties and check whether ISSRs in the Arctic are very thick and present only in winter. For this purpose we use high-resolution radiosonde data from four launch stations in the Arctic circle. The data sources and handling are described in the next section. Results are presented in Section 3 and some discussion is provided in Section 4. Summary and conclusions are given in the final Section 5.

2 Data and their treatment

We use radiosonde data from arctic launch stations that belong to the Global Climate Observing System (GCOS) Reference Upper-Air Network (GRUAN Bodeker et al., 2016). The selected stations, their coordinates and the temporal coverage of the data used are compiled in Table 1. The location of these stations in the Arctic circle can be seen as well in Figure 1. More specifically, the data belong to the special data product RS92-GDP.2. All these data are obtained from a single radiosonde type, Vaisala RS92-SGP, involving identical calibration and ground-check procedures. All data are identically processed. This assures that time series are homogeneous and that measurements of all GRUAN stations are equivalent. The GRUAN processing is described in Immler et al. (2010); Dirksen et al. (2014).

We use the single profiles for some time series, but we compute as well monthly and overall averages, standard deviations, and other quantiles. Months with less than 15 profiles at a station are not considered for the computation of monthly statistics.

Profiles are considered valid when they contain only valid numbers and no NaNs (NaN: not a number). The GRUAN data contain temperature, pressure and altitude of the thermal tropopause (according to the WMO definition). Occasionally temperature inversions in the mid troposphere are falsely interpreted by the GRUAN processing as the tropopause. These profiles are detected when ISSRs appear at unrealistically high distances (more than 50 hPa) above the tropopause; they are considered invalid and not used for the analyses.

In this paper we constrain ourselves to altitudes with temperatures below 235 K in order to avoid the counting of air inside supercooled liquid or mixed phase clouds as ice-supersaturated regions. Ice supersaturation is only counted when the air is not already supersaturated directly at the 235 K isotherm because this might still be the top of a supercooled liquid cloud. 235 K is approximately the lowest temperature to which cloud droplets can be supercooled before they eventually freeze. In effect, our analysis refers to the cold layers of the atmosphere where only two states of pure water are possible, vapour or ice.

There is a pecularity for Eureka. Occasionally there is a strong temperature inversion at the ground and

Table 1: GRUAN stations used for the study. Note that all data series have minor or major gaps.

Site	SOD	NYA	BAR	ERK
name	Sodankylä	Ny-Ålesund	Barrow	Eureka
state/country	Finland	Svalbard, Norway	Alaska, USA	Nunavut, Canada
WMO station no.	02836	01004	70027	71917
longitude	26.63° E	11.93° E	156.61° W	85.93° W
latitude	67.37° N	78.92° N	71.32° N	79.98° N
elevation (m)	179	5	8	10
data used	2007–2019	2006–2018	2009–2018	2008–2017
no. of valid profiles	2437	2668	3055	4775

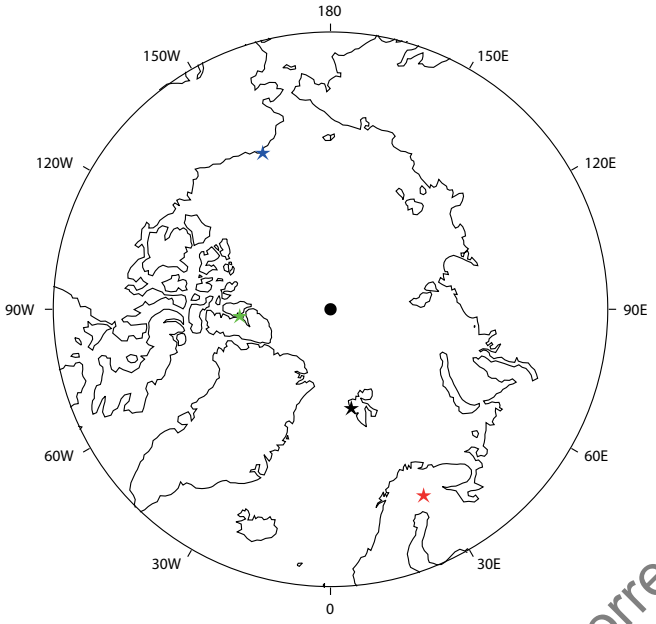

Figure 1: Map of the Arctic showing the four radiosonde launch sites considered in this study (stars): Sodankylä (red), Ny-Ålesund (black), Barrow (blue), and Eureka (green). The black dot in the middle represents the north pole.

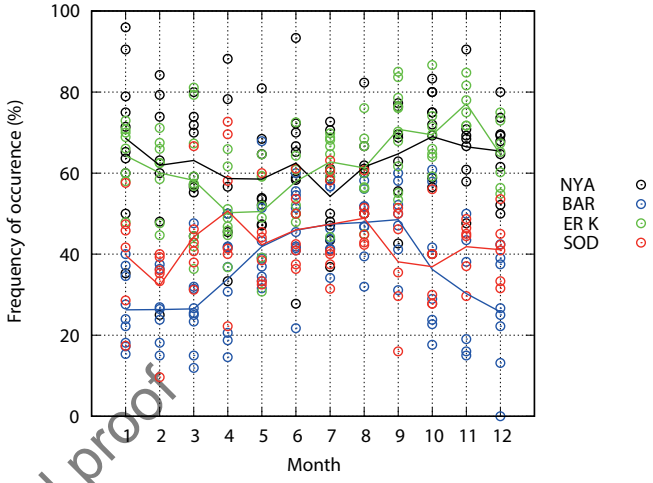

Figure 2: Monthly frequencies of occurrence of ISSRs over the four Arctic sites (see key). The variability is large and there is no obvious seasonal variation. Results for individual months in an individual year are presented as circles, the mean annual variation for each station is given as the solid lines.

the reduced vertical mixing of the air favours increasing relative humidity accompanied with ice supersaturation, haze, fog, and a cloud layer at the surface. In order to avoid such cases in our study we use an additional pressure constraint (for all stations) and count only events where the pressure of the lower boundary is below 600 hPa. ISSRs at the ground might be considered a curiosity, but in fact the first recording of ice supersaturation in the atmosphere was from a hair hygrometer measurement in a weather hut on greenland, performed by Alfred Wegener in 1906 (Wegener, 1914).

The 1-Hz resolution of the measurements implies a vertical resolution of the profiles of a few metres. Such high resolution is achieved in spite of instrumental inertia growing with decreasing temperature by modelling the measurements as passed though a low-pass filter and subsequent deconvolution. The process is described in the paper by Dirksen et al. (2014).

3 Results

3.1 Frequency of ice supersaturation, annual variability, trends

Figure 2 shows for each month (i.e. January to December) the fraction of radiosonde profiles that contained ice-supersaturated layers. Months with less than 15 profiles at a station have not been considered. There are some months with only a few ISSRs (or even none at all), in particular at Barrow and Sodankylä, but as well other months where more than 90 % of the profiles have ice supersaturation, in particular at Eureka and Ny-Ålesund. In all months the highest frequency of occurrence is either over ERK or NYA, while the lowest is over BAR or SOD. The means over all monthly values are given as lines in the figure for the four stations. The mean frequency of ocurrence has a summer maximum at BAR, but at ERK the maximum is rather in fall. The mean annual variation is small at SOD and NYA. The mean (over all months) frequency of occurrence of ice-supersaturation is 43 % at SOD and 36 % at BAR, but it is substantially higher with 63 % at NYA

Table 2: Summary table of average properties of ISSRs over the Arctic circle. SOD: Sodankylä, NYA: Ny-Ålesund, BAR: Barrow, ERK: Eureka. IQR is the interquartile range, WVMR is the water vapour volume mixing ratio. The line 'mean thickness" gives the mean plus/minus one standard deviation.

Site	SOD	NYA	BAR	ERK
no. of ISSRs	1973	4318	2083	8802
fraction of ISSRs	0.81	1.62	0.68	1.84
mean thickness (m)	216±250	374±530	218±259	325±454
median thickn. (m)	125	172	130	150
IQR (m)	56-289	68-445	57-281	63-396
total range (m)	3.32–2760	3.23–4883	3.70–2530	3.04–4891
geom. mean μ	4.82	5.16	4.85	5.04
geom. std. dev. σ	1.19	1.34	1.14	1.32
altitude range (m)	4196–12623	3495–13974	3724–13355	3487–12217
rel. pres. range (hPa)	−29–326	−44–456	−20–296	−45–351
min temp. (°C)	−76	−83	−75	−78
WVMR range (ppmv)	7–504	3–488	8–500	5–479

and 62 % at ERK. There is more ice supersaturation at the more northern sites.

The frequencies of occurrence show (so far) no long-term trends. The seasonal cycles at the four locations are not very clear but there is a tendency for higher values in summer and lower ones in winter for SOD and BAR and for the reverse cycle in NYA and ERK. In Figure 2 it appears that the range from the lowest to the highest frequency of occurrence is wider in winter (<10% to >90%) than in summer (in July from about 30 % to 70 %).

3.2 Thickness of ice supersaturated layers

The thickness of ice-supersaturated layers was studied in several papers before (Spichtinger et al., 2003b; Rädel and Shine, 2007; Dickson et al., 2010b). The resulting mean thickness values were quite different and it seems that they depend on the vertical resolution of the data. While Spichtinger et al. (2003b) found for Lindenberg, Germany, a mean of 560 m using data with vertical resolution of about 30 m, Treffeisen et al. (2007) (for Ny-Ålesund) and Rädel and Shine (2007) (for southern England) found considerably larger values of 600 m to more than 2 km with data of coarse altitude resolution of the order 200–300 m. The resolution dependence of these results is apparent from a study by Dickson et al. (2010b) who used data from British Isles like Rädel and Shine (2007), but with a high vertical resolution of about 10 m; they found average thicknesses of the order 100 to 200 m. The resolution dependence of the thickness results will be shown below using the current data.

The thickness distribution is obtained in the following way: First a cumulative distribution is determined from all thickness data, then a kernel density estimate (Epanechnikov kernel, with variable bandwidths from 33 to 47 m) is applied to obtain the probability density function. These functions are displayed in Figure 3. The results can be summarised in a few characteristic values, which are given in Table 2. In agreement to earlier

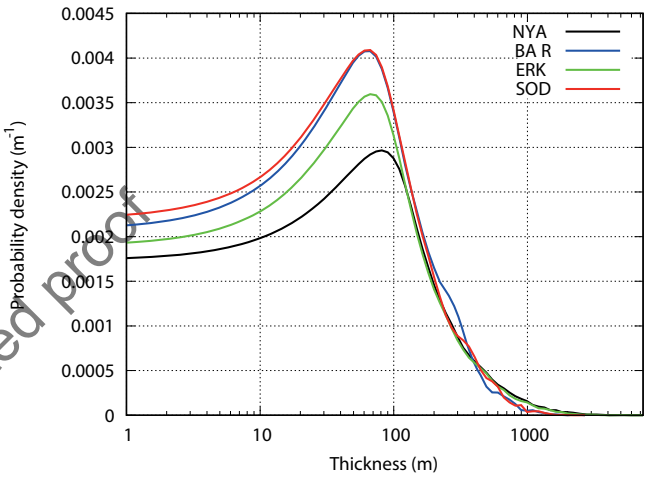

Figure 3: Probability density (pdf) of ISSR layer thickness at all arctic stations. All pdfs peak at thickness values below 100 m.

studies we find very skew distributions. Mean values are of the order 200 to 400 m, the standard deviations exceed the means in all cases, a signature for skewness. In fact, the moment coefficient of skewness is 2.69 for SOD and exceeds 3 in all other cases. Minimum thicknesses are of the order of a few metres, but maximum thicknesses can exceed several kilometres; in particular the northernmost stations NYA and ERK have maxima approaching 5 km. Such thick ISSRs have not been reported before to our knowledge.

It seems possible to fit log-normal distributions to the data (red curves in Figure 4). The fits are excellent for the bulk of the distributions but they don't fit quite well all upper tails and the lower tails in the case of the northern stations NYA and ERK. Corresponding geometric means, μ, and geometric standard deviations, σ, are given in Table 2. Although the number of data and thus the statistical robustness in the tails are quite low, we believe that the log-normal model is not appropriate for the highest thickness values. Spichtinger et al. (2003b) fitted a pair of Weibull distributions to corre-

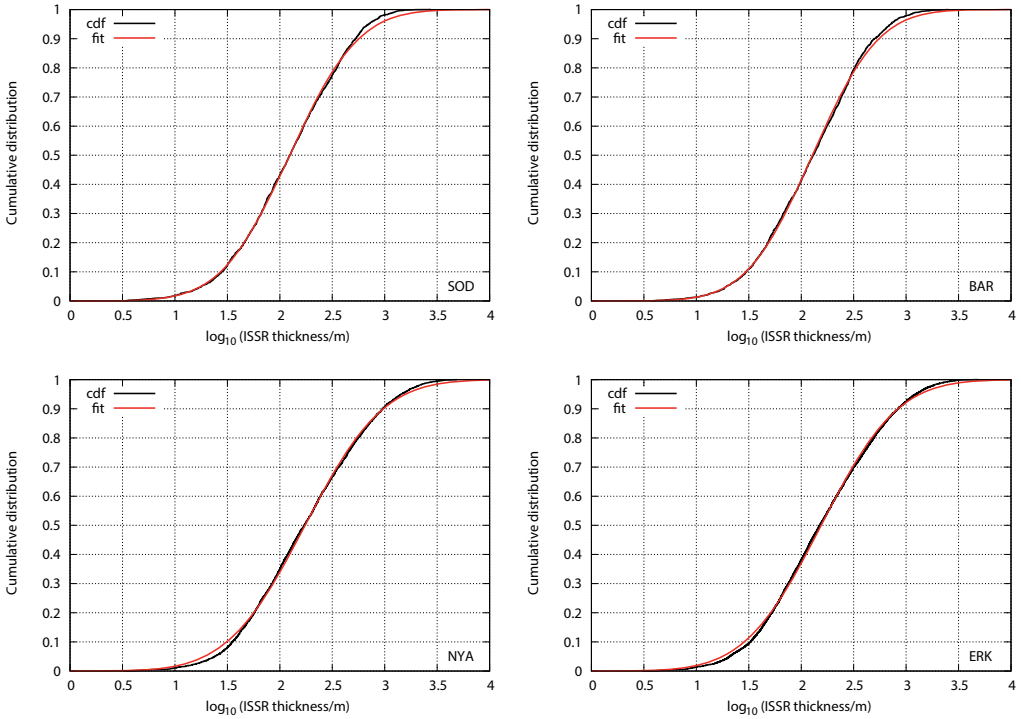

Figure 4: Cumulative probability distributions (black) of ISSR layer thicknesses at SOD (top left), BAR (top right), NYA (bottom left), and ERK (bottom right). The red lines in each panel are fitted log-normal distributions.

sponding thickness data with a change of the coefficients at a thickness of about 1000 m. The fact that the best-fit log-normal distribution does not match the upper tail leads to quite large differences when we compute the arithmetic mean and standard deviation from its geometric counterparts. The log-normal is thus an excellent model for the thickness distribution below about 1000 m, but for the very thick ISSRs this model meets its limits. It is conceivable that the "bulk" thickness distribution is produced by multiplicative growth processes where the relative growth rate is independent of the current thickness of an ISSR. For the very thick specimen there must then be either different growth processes at work or limitations begin to act that are not essential for thin ISSRs.

For the far northern stations NYA and ERK there is a strong seasonal variation of the average layers thickness, as Figure, 5 clearly shows. The amplitude of this variation is about 2. In contrast, no such variation is apparent for SOD and BAR. The fact that ISSRs are thickest in the polar night at NYA and ERK, which extends from the end of october to the end of february at these locations, hints at radiative cooling as the main cause of the thickness maximum.

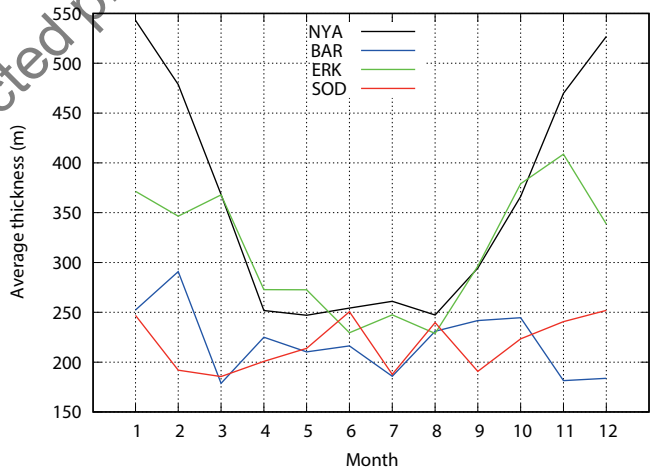

Figure 5: Seasonal variation of the average thickness of ice supersaturated layers at four arctic stations as indicated.

3.3 Altitude of ISSRs, absolute and relative to the tropopause

Altitudes where ISSRs occur vary substantially and show a strong seasonal variation. Figure 6 shows the altitudes of the upper boundaries of ISSRs over the arctic stations ranging from about 4000 m to almost 14000 m. Winter values are lower, summer values higher, the seasonal variation is considerably stronger than the daily (synoptic) variation. The variation is similar for the lower boundaries (not shown). The seasonal altitude variation reflects the corresponding variation of the tropopause height. Figure 7 shows the pressures at ISSR tops (for the bottoms the figures are similar and thus not shown), relative to the tropopause pressure. Obviously the tropopause is a quite strong upper limit for ice supersaturation; most ISSRs are located immediately below the tropopause and ISSRs in the stratosphere are rare exceptions. This agrees with results obtained from

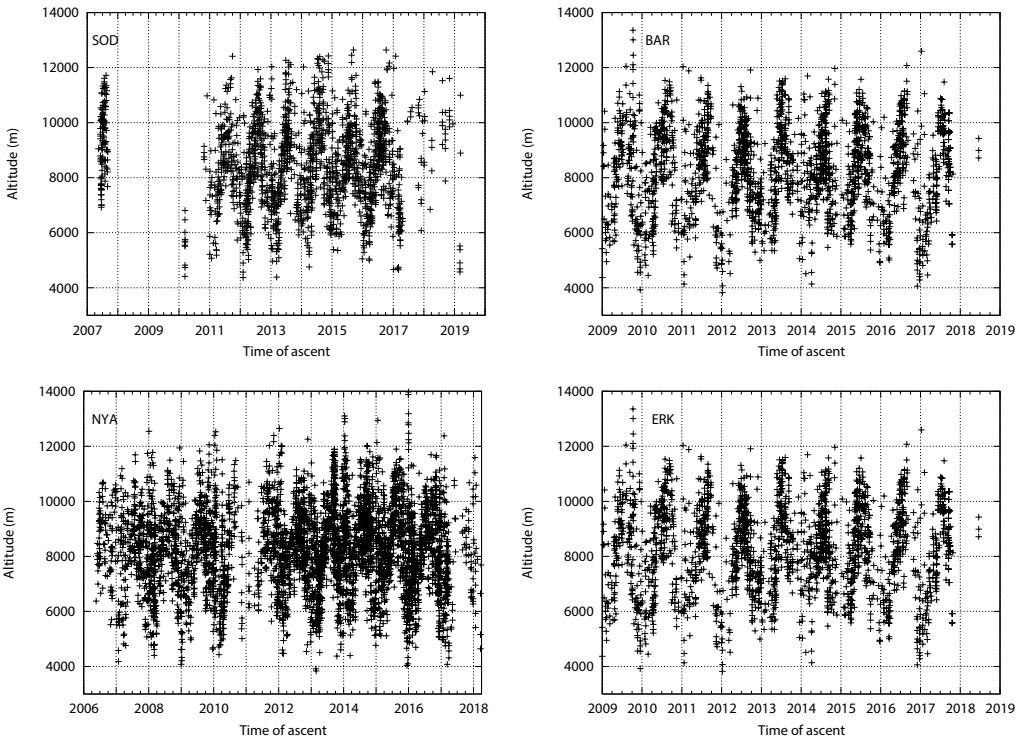

Figure 6: Altitudes of the upper boundaries of ice supersaturated layers over arctic stations SOD (top left), BAR (top right), NYA (bottom left), and ERK (bottom right).

commercial aircraft data (Neis, 2017) since 1995 in the MOZAIC (Measurements of OZone and water vapour by in-service AIrbus airCraft, Marenco et al., 1998; Helten et al., 1998) and IAGOS (In-service Aircraft for a Global Observing System, Petzold et al., 2015) projects.

Figure 7 shows a clear seasonal cycle as well. ISSRs are located between the tropopause and a level about 100 hPa below it in summer, but in winter they occupy a much deeper region, down to about 250 to 300 hPa below the tropopause, where the layer depth is larger at NYA and ERK than at BAR and SOD. For satellite data of upper tropospheric humidity with coarse vertical resolution this might be misinterpreted as the occurrence of very thick arctic ISSRs in winter.

3.4 Temperature and absolute humidity in ISSRs

The distributions of the temperatures at the tops and bottoms of the ISSRs are shown in Figure 8. Because of our temperature constraint, the maximum temperature in the studied ISSRs is 235 K (−38 °C). The lowest temperatures are below −80 °C, but such low temperatures occur rarely. Most ISSRs have temperatures between −40 and −60 °C and the temperature difference between their tops and bottoms is on average about 2–3 K; occasionally the difference substantially exceeds 10 K, when the ISSRs are very thick, and ISSRs in the lowermost stratosphere have a higher temperature at the top than at the bottom since the temperature increases upward in the stratosphere. As expected, ISSRs at the far northern stations NYA and ERK are on average colder than the ISSRs at SOD and BAR.

Absolute humidity, expressed as volume mixing ratio (WVMR), ranges from about a few (3–8) to $(450–500) \times 10^{-6}$ (ppmv), with peak frequencies of occurrence at less than 100 ppmv, see Figure 9. The minima are typical for the tropopause and the lowermost stratosphere. On average, mixing ratios are lower at the far northern stations NYA and ERK than at SOD and BAR.

3.5 Relation between thickness and maximum supersaturation

There is a certain correlation between the maximum supersaturation and the thickness of an ISSR, as one might expect. Figure 10 shows the single data pairs as crosses and average lines to guide the eye. Evidently, the very thick ISSRs all have maximum supersaturation values exceeding 10 or even 20 % and the largest maxima reach and exceed 50 % for thick layers. Such high values occur in thin ISSRs as well, but low maxima of the order of a few percent occur only in thin ISSRs. The average tendency is that higher maxima are to be expected in thicker ISSRs, but high maxima occur in thin ISSRs as well. One might rather say, that high maxima occur at all thickness values, and the average upward tendency has its origin mainly in the lack of low maxima in thick ISSRs. It makes no sense to report linear correlation coefficients since the average “correlation” is non-linear.

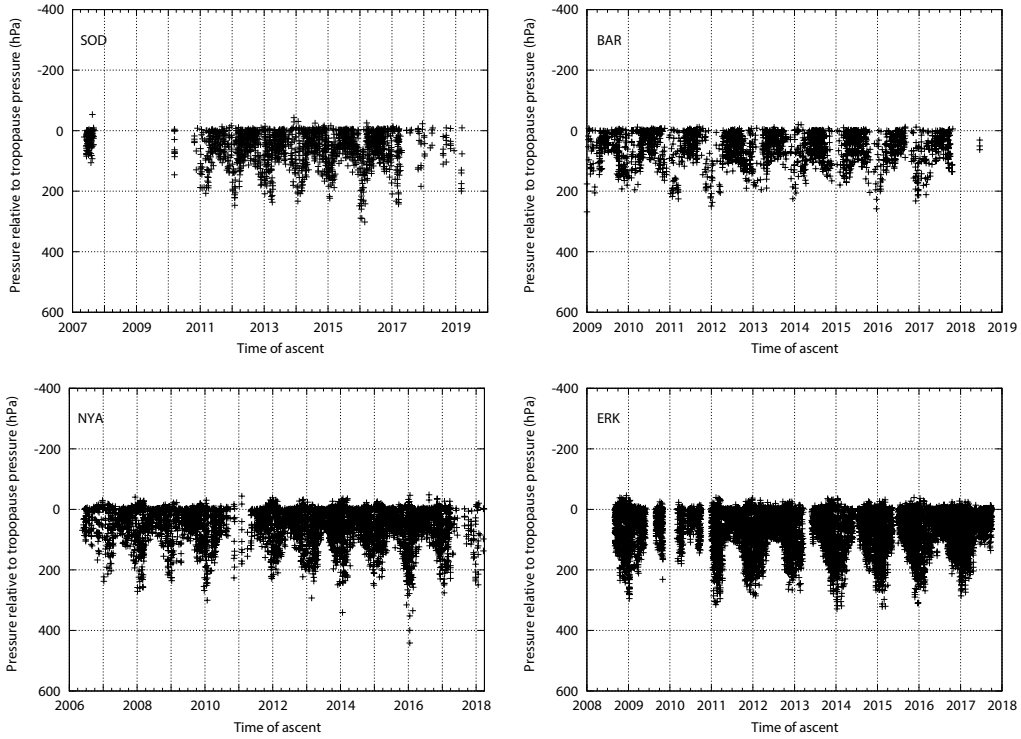

Figure 7: Pressures of the upper boundaries of ice supersaturated layers over arctic stations SOD (top left), BAR (top right), NYA (bottom left), and ERK (bottom right). Most ISSRs are located directly below the tropopause. But the altitude region where ISSRs occur extends to considerable lower levels in winter than in summer.

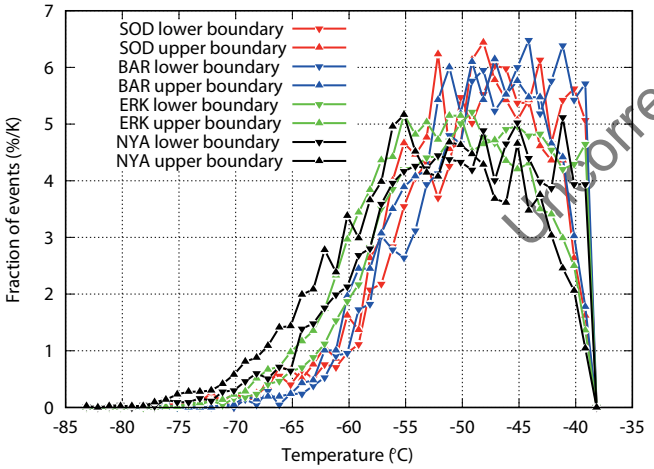

Figure 8: Temperatures of the upper and lower boundaries of ice supersaturated layers over four locations in the Arctic.

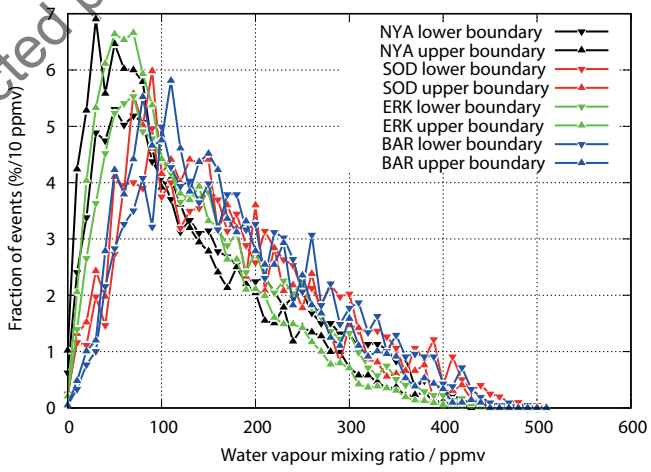

Figure 9: Water vapour volume mixing ratios (nmol per mol or ppmv) of the upper and lower boundaries of ice supersaturated layers over four locations in the Arctic.

There is neither correlation between thickness and temperature nor between thickness and relative pressure.

3.6 Stacking of ISSRs

It happens quite frequently that a single radiosonde profile shows more than one ice-supersaturated layer. For the northern stations NYA and ERK this seems to be the rule rather than the exception, because for these sets of profiles the fraction of ISSRs (that is the number of ISS layers divided by the number of valid profiles) exceeds unity; see Table 2. Figure 11 shows the relative frequency of ISSR stacks at the 4 arctic stations. Single ISSRs occur most often but double ISSRs occur with only slightly smaller frequency. The maximum number of ISSRs in a single profile is 9 for SOD, 11 for BAR, 13 for NYA and even 14 for ERK. Again it appears that there is a latitudinal gradient with larger stacking numbers at the more northern sites.

Overall it appears from Figure 11 that it is possible to fit a straight line through the tops of the histogram lines. In a half-logarithmic plot with discrete values on the abscissa this indicates a geometric distribution. Geometric ditributions, the discrete counterparts of exponential

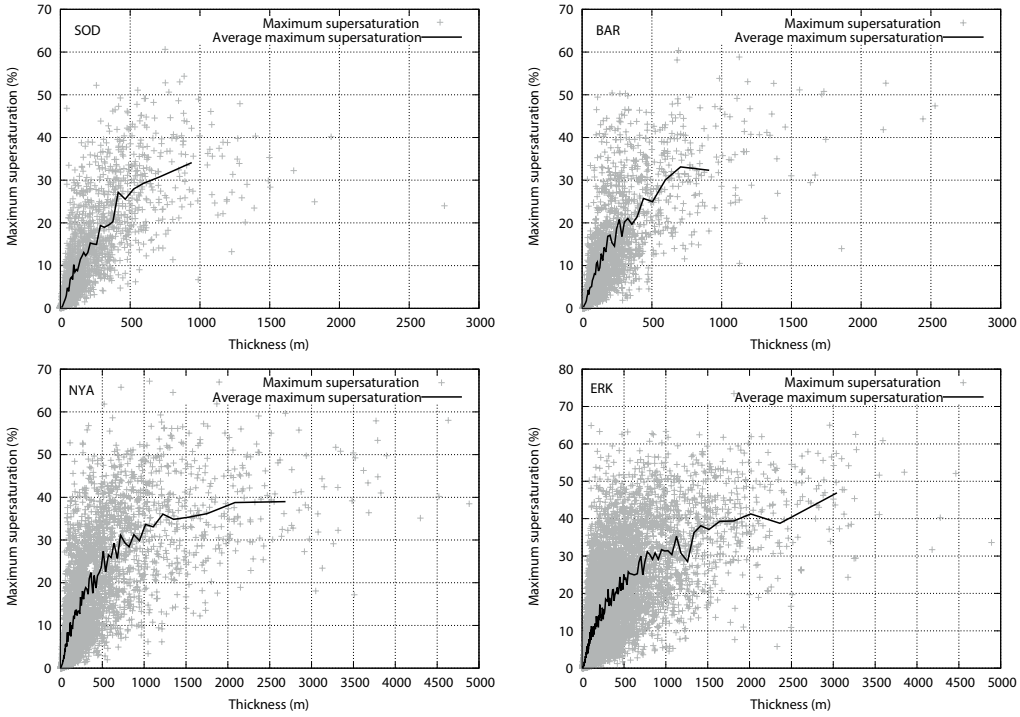

Figure 10: Maximum supersaturation, that is $\max(RH_i - 100\,\%)$, vs. thickness (crosses) of ice supersaturated layers over arctic stations SOD (top left), BAR (top right), NYA (bottom left), and ERK (bottom right). The thick black line in each panel is the average of the maximum supersaturation values over thickness intervals appropriate to each data set. Note the different scales.

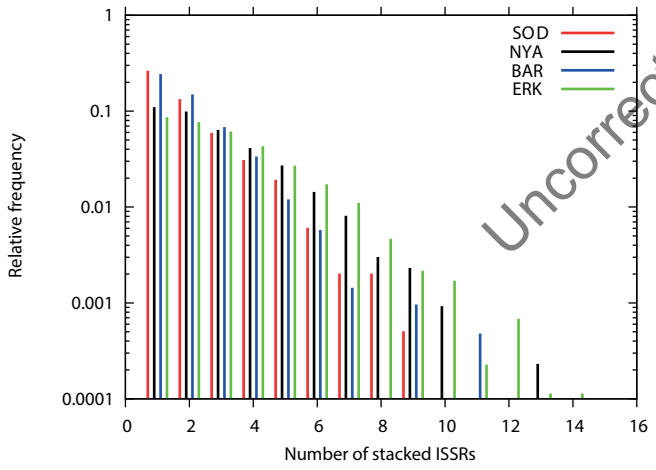

Figure 11: Relative frequency of the number of stacked ISSRs for radiosonde profiles obtained over arctic stations SOD (red), NYA (black), BAR (blue), and ERK (green).

distributions, are characterised by a single parameter, which is the inverse of the respective mean value. The value of this parameter is 0.52 for the more southern stations SOD and BAR and 0.37 for NYA and 0.33 for ERK. Again, there is a distinctive difference between the high arctic and the more moderate arctic. A geometrical distribution is memoryless, which means in the present case that the probability to find another supersaturated layer in a profile is independent of the number already found. This implies that these layers should often appear independently of each other.

4 Discussion

When one compares the present results with those of Spichtinger et al. (2003b) who analysed ice supersaturation using radiosonde data from Lindenberg (Germany, 52.21° N, 14.12° E, 98 m) one finds agreement for certain parameters, but also differences. For instance, temperatures of ISSRs are mostly lower than −40 °C in the Arctic ISSRs as well as over Lindenberg. The ISSRs occur mainly in an about 200 hPa thick layer beneath the tropopause with a distinct annual cycle (that is, the layer is thickest in winter and shallowest in summer). The thickness distribution of single ISSRs shows a break at about 1 km in the Lindenberg data set, while in the present study we find that the log-normal fit to the thickness distribution, being excellent for smaller thicknesses, fails at values exceeding about 1 km. The results differ quite much regarding the frequency of occurrence of ISSRs. In Lindenberg there were 730 ISSRs in 437 profiles out of a total of 1563, that is, the fraction of ISSRs is 0.47 in this data set (730/1563, note that in the paper the authors state the fraction of profiles that contain an ISSR, i.e. 437/1563 or 0.28). Table 2 gives much larger fractions of ISSR for the arctic stations, with values increasing with latitude. SOD and BAR both have still fractions below unity, but for the high arctic locations NYA and ERK the ISSR fractions are closer to two than to one, which means that there are quite often several ISSRs stacked on top of each other in the arctic troposphere. The numbers for Lindenberg show that this happens there as well, but ice supersaturation seems much less frequent in Lindenberg than in

the arctic. This is consistent with results from satellite data (Gierens et al., 2004). It might be that very shallow ISSRs were undetected in the Lindenberg data, so the difference between the mid-latitude and the arctic data may actually be smaller than the data suggest. Thus, the effects of vertical resolution are considered next.

4.1 Effects of vertical resolution

The vertical resolution of the radiosonde data has a considerable influence on the resulting estimates for the mean thickness. This influence can be tested when the data are smoothed to a lower resolution before performing the calculations. We did this for the SOD data. Instead of the data in full 1 Hz resolution we used the median values of groups of 20 consecutive data, in an attempt to simulate a 0.05 Hz resolution. Obviously, with such a resolution it is not possible to detect ISSRs that are only a few metres thick. Accordingly, the minimum thickness increases from 3.3 m to more than 40 m (there is no exact value, the number depends on which subset of data is actually selected). The median value increases from 125 to about 230 m. The reduced resolution has also an effect on the maximum stacking number which is reduced from 9 to 5 or 6.

The inertia of a sensor can be simulated by backward Gaussian filtering, that is the actual value at a certain altitude is modelled as a weighted sum of a number of values measured before. Here we use a Gaussian filter with 21 points and a sigma of 10 s. Note that in contrast to the median smoothing all data are used here (apart from edge-truncation). Thus the minimum thickness is still very small, 3.7 m. However, the thickness distribution is shifted to higher values as well. The median thickness is 173 m and the IQR is 84 to 373 m; these values are considerably higher than without filtering (see Table 2). The maximum number of stacked ISSRs is reduced to 7.

Nadir sounders on satellites have a low vertical resolution. Kempter (2016) looked for ISSRs in data from the High Resolution Infrared Sounder (HIRS). She found them only north of 55° (the study was constrained to the northern hemisphere) and only in the cold season but not in summer. In contrast, the radiosonde data show ISSRs throughout the year in the northern latitudes. The contradiction is probably the result of the low vertical resolution of the satellite data in combination with the seasonal variation of the depth of the layer beneath the tropopause where ISSRs occur. We have seen that this layer is much thicker in winter (250–300 hPa) than in summer (100 hPa). Hence the probability to detect ice supersaturation with a nadir sounder is much larger in winter than in summer and it seems that the layer is generally too shallow in summer for HIRS to detect any ice supersaturation.

There is still another effect of vertical resolution. Petzold et al. (2019) compare the frequency of occurrence of ISSRs in IAGOS and MOZAIC data (that is, local measurements of relative humidty, averaged over 30 hPa thick layers) with the frequency of occurrence of cirrus clouds obtained from satellite data. As ice supersaturation is a condition for cirrus formation one should expect a higher coverage of ISSRs than of cirrus clouds, unless the latter survive for many hours in subsaturated air. But surprisingly, CALIPSO (Cloud-Aerosol Lidar and Infrared Pathfinder Satellite Observations) shows a higher cirrus coverage than IAGOS/MOZAIC find for ISSRs. This observation can be explained when we take into account our current result that ISSRs are often stacked, that is, ISSRs occur in several altitudes simultaneously. The commercial aircraft, measuring locally, registers only one of these ISSRs, but when cirrus clouds form in several altitudes CALIPSO finds a larger cirrus coverage if the ISSRs and cirrus clouds do not completely overlap vertically. The radiosonde data thus provide an explanation for this phenomenon. Petzold et al. (2019) do not report whether the coverage difference between cirrus and ISSRs depend on latitude, but as there is increasing stacking of ISSRs towards the high latitudes, we expect that the coverage difference should increase as well.

4.2 Effects of measurement uncertainties

Dirksen et al. (2014) lists the types and origins of measurement errors for the RS92 radiosonde. The GRUAN processing removes these errors as far as possible and collects and reports all uncertainties (to each single measurement, that is, the uncertainties are presented as profiles along with the measurements). Comparisons obtained from simultaneous launches of GRUAN radiosondes together with frost point hygrometers (Dirksen et al., 2014, figure 17) indicate that the GRUAN data may suffer from a dry bias at temperatures below −40 °C, that is, in the regions relevant to the present study. The test locations include Sodankylä. This implies that ice-supersaturation might even be more frequent than what has been found here.

Capacitive humidity sensors like that of the RS92 radiosonde get slow when the ambient temperature falls below about −40 °C, that is, they react with a delay (time lag) to changes of the ambient humidity while rising through the air. The time lag of the humidity sensor could be a problem as well. In the temperature regime below −40 °C the time lag exceeds 20 s and it increases to minutes towards lower temperatures. The GRUAN processing corrects for this, and applies a low-pass filter in order to suppress noise. The result of the growing inertia of the sensor could be that thin ISSRs are not found at high altitudes (low temperatures). If the time-lag problem leads to excessive smoothing of the RHi profiles, thin ISSRs should occur more often at lower altitudes and should get rare at higher altitudes. That is, there should be a (positive) correlation between layer thickness and altitude, but this is not the case. These correlations are negative and of small magnitude for all stations. This result corresponds to the absence of correlation between layer thickness and temperature reported above. It seems thus that the time-lag correction works

well such that the analyses of the thickness distributions yields valid results.

The measurement uncertainties affect the estimates of layer thicknesses and frequencies of occurrence as well. As worst case scenarios we studied the effect of adding or subtracting the uncertainty of relative humidity to the nominal data, that is, we consider the effect of using $RH + u\_RH$ and $RH - u\_RH$ instead of RH. This check is performed for SOD only. First, the number of detected layers changes quite substantially: Instead of 1973 ice-supersaturated layers we find 1588 and 2239, respectively. This strong variation implies that parts of the profiles are very close to ice saturation. The thickness distribution is affected as well, but the shape of the distribution is still approximately log-normal. Instead of a median thickness of 125 m we get 113 and 147 m, respectively; that is, the effect of measurement uncertainties on the thickness distribution is not very strong. Finally, the stacking numbers are affected. While there is still a maximum of 9 stacked ISSRs in the $RH + u\_RH$, the maximum increases to 11 in the $RH - u\_RH$ case, which implies that a larger ISS layer is broken into two adjacent layers.

4.3 The role of the arctic tropopause

We saw that the thermal tropopause is a quite strong upper limit of the region where ice-supersaturation occurs; it occurs rarely above the thermal tropoause. It is thus appropriate to consider the climatology of the arctic tropopause pressure and temperature. A prominent feature of the arctic tropopause is a pressure maximum at about 90° W, that is the direction to ERK. This maximum is strongest with pressures exceeding 325 hPa in spring. At the position of ERK, the seasonally averaged tropopause pressure stays at about 300 hPa in summer and fall and it is lowest in winter at about 280 hPa. This seasonal variation is reflected in the ISSR frequency of occurrence (see Figure 2) at ERK with a minimum in spring and a maximum in winter. BAR has the maximum frequency of ISSR occurrence in summer, and indeed the average tropopause pressure at BAR is lowest in summer. However, a quite large winter-to-spring increase of tropopause pressure from about 245 hPa to more than 300 hPa at NYA has barely an effect on the ISSR frequency. Instead the avarage layer thickness (see Figure 5) changes by a factor of two. At ERK the layer thickness decreases as well when simultaneously the average tropopause pressure increases from its winter low to its spring high. Tropopause pressure variations are moderate at SOD, and so are seasonal variations of both ISSR frequency and layer thickness at that site. These behaviours are by and large too inhomogeneous to base firm conclusions on them.

Contrary to climatological tropopause pressure variability, the corresponding tropopause temperature is quite homogeneous throughout the arctic circle with differences not exceeding 2 K. Tropopause mean temperatures are around −56° to −57 °C in winter and about −48° to −50 °C in summer. As we consider 235 K (−38 °C) the upper temperature limit of ISSRs, and since the tropopause is a quite sharp upper limit of ISSR occurrence, there is on average a larger temperature range in winter where ISSRs can exist than in summer. This might explain the strong seasonal cycles of ISSRs altitudes and of tropopause-relative pressures evident in Figures 6 and 7.

4.4 Limits of the log-normal distribution model

Many growth processes in nature lead to log-normal size distributions (Limpert et al., 2001), which appears for instance as a result of many independent growth (or shrinking) events that act multiplicatively, that is, they change size by factors that are independent of the current size, and where no single growth or shrinking event dominates. This is analogous to additive processes that lead to a normal distribution according to the central limit theorem. Unfortunately, what such a multiplicative process could be in the case of ISSR layer growth and shrinking, is not known currently.

Vertical growth of ISSRs by lifting is constrained. As soon as the critical supersaturation for homogeneous ice nucleation is reached clouds form and the supersaturation starts to be consumed by crystal growth. Lifting can thus lead to a clear ISSR between the level where ice saturation is reached and the level where the critical supersaturation is reached. The corresponding thickness, i.e. the distance between these two levels, does not exceed, say, 600 m (Gierens et al., 2012, their figure 9.6). That is, thicker ISSRs are connected to other processes than lifting, e.g. cloud formation, or radiative cooling in cold dark winter months without sunlight. This may explain why the log-normal model for the thickness distribution breaks down at high values.

5 Summary and conclusions

We have studied high-resolution quality-controlled radiosonde data for 4 launch stations in the Arctic that belong either to the GRUAN network (SOD, BAR, NYA) or that used GRUAN processing (ERK). The focus of the study is ice-supersaturation, a thermodynamic state that is required for cirrus to form and for contrails to persist. On average, ice supersaturation occurs in about 40 % of the profiles in SOD and BAR, but in more than 60 % of the profiles in the high Arctic locations NYA and ERK. It appears that the frequency of ice supersaturation increases with the geographic latitude. There are weak seasonal cycles of the occurrence frequency, with a phase reversal betweem SOD and BAR on the one and NYA and ERK on the other hand. A decadal trend is not apparent. Stacked ISSRs (that is, more than one ISSR in a single profile) occur quite often, for the far northern locations NYA and ERK this is the rule rather than the exception.

Vertical extensions of arctic ISSRs range from a few metres to almost 5 km. In fact, the NYA and ERK data contain the thickest ISSRs we have so far seen. However, it turns out that ISSRs average thicknesses have been overestimated in past studies because the data underlying them had much lower vertical resolution than the GRUAN data. Median thicknesses are of the order 100–200 m, and the bulk of the thickness data can be fitted with log-normal distributions quite well. The log-normal model fails at the upper tail of the thickness distribution. Probably, different physical processes act or are predominant in thinner than 1 km and thicker ISSRs, respectively. For the far northern locations NYA and ERK we find a strong seasonal cycle of the average layer thickness, but no such variability at SOD and BAR. The thickness maxima at NYA and ERK occur in the polar night, which suggests radiation cooling to be the mechanism leading to ice supersaturation and thickening the layers.

Like in mid-latitudes, arctic ice supersaturation occurs most frequently directly beneath the tropopause. The layer where ISSRs occur displays a strong seasonal thickness variation. In summer it extends about 100 hPa below the tropopause, but in winter the layer reaches down 200 to 300 hPa below that level. This variation explains why an infrared sounder like HIRS detected ice supersaturation only in winter in the study of Kempter (2016).

Temperatures in arctic ISSRs are mainly in the range −40 to −60 °C, but can as well be lower than −70 °C. Water vapour volume mixing ratios range from a few ppmv typical for the tropopause to about 500 ppmv and the relative humidity with respect to ice can reach maximum values of 150–160 % (and occasionally even higher). There is a weak (non-linear) correlation of maximum supersaturation and thickness of ISSRs. Temperature and absolute humidity seem not correlated with ISSR thickness.

Ice supersaturation can occur at the ground in the Arctic, probably often in combination with ice fog or diamond dust.

Acknowledgments

This work was done while L. Wilhelm visited DLR for practical training. The data used in this study have been provided by the GRUAN network and by Environment and Climate Change Canada. A discussion session of KG with colleagues (Matrixgruppe Wasserdampf) yielded valuable ideas that found their way into the manuscript. We thank Stefan Kaufmann for checking the manuscript. The data set of GRUAN-RS92.2 has an own DOI: Sommer, Michael; Dirksen, Ruud; Immler, Franz. (2012): RS92 GRUAN Data Product Version 2 (RS92-GDP.2). GRUAN Lead Centre. DOI: 10.5676/GRUAN/RS92-GDP.2

References

Alraddawi, D., A. Sarkissian, P. Keckhut, O. Bock, S. Noël, S. Bekki, A. Irbah, M. Meftah, C. Claud, 2018: Comparison of total water vapour content in the arctic derived from GNSS, AIRS, MODIS and SCIAMACHY. – Atmos. Meas. Tech. **11**, 2949–2965, DOI: 10.5194/amt-11-2949-2018.

Bodeker, G., S. Bojinski, D. Cimini, R. Dirksen, M. Haeffelin, J. Hannigan, D. Hurst, T. Leblanc, F. Madonna, M. Maturilli, A. Mikalsen, R. Philipona, T. Reale, D. Seidel, D. Tan, P. Thorne, H. Vömel, J. Wang, 2016: Reference upper-air observations for climate: From concept to reality. – Bull. Amer. Met. Soc. **97**, 123–135, DOI: 10.1175/BAMS-D-14-00072.1.

Dickson, N., K. Gierens, H. Rogers, R. Jones, 2010a: Probabilistic description of ice-supersaturated layers in low resolution profiles of relative humidity. – Atmos. Chem. Phys. **10**, 6749–6763.

Dickson, N., K. Gierens, H. Rogers, R. Jones, 2010b: Vertical spatial scales of ice supersaturation and probability of ice supersaturated layers in low resolution profiles of relative humidity. – In: R. Sausen, P. van Velthoven, C. Brüning, and A. Blum (Eds.), Proceedings of the 2nd International Conference on Transport, Atmosphere and Climate, DLR Forschungsbericht 2010-10, 239–243.

Dirksen, R., M. Sommer, F. Immler, D. Hurst, R. Kivi, H. Vömel, 2014: Reference quality upper-air measurements: GRUAN data processing for the Vaisala RS92 radiosonde. – Atmos. Meas. Tech. **7**, 4463–4490.

Gierens, K., R. Kohlhepp, P. Spichtinger, M. Schroedter-Homscheidt, 2004: Ice supersaturation as seen from TOVS. – Atmos. Chem. Phys. **4**, 539–547.

Gierens, K., P. Spichtinger, U. Schumann, 2012: Ice supersaturation. – In: U. Schumann (Ed.), Atmospheric Physics. Background – Methods – Trends, Springer, Heidelberg, Germany, chapter 9, 135–150.

Hallar, A., L. Avallone, R. Herman, B. Anderson, A. Heymsfield, 2004: Measurements of ice water content in tropopause region arctic cirrus during the SAGE III Ozone Loss and Validation Experiment (solve). – J. Geophys. Res. **109**, D17203, DOI: 10.1029/2003JD004348.

Hassol, S., 2004: ACIA, Impacts of a warming Arctic: Arctic Climate Impact Assessment – Cambridge University Press, Cambridge, UK, 26 pp.

Helten, M., H.G.J. Smit, W. Sträter, D. Kley, P. Nedelec, M. Zöger, R. Busen, 1998: Calibration and performance of automatic compact instrumentation for the measurement of relative humidity from passenger aircraft. – J. Geophys. Res. Atmos. **103**, 25643–25652, DOI: 10.1029/98JD00536.

Heymsfield, A., L. Miloshevich, C. Twohy, G. Sachse, S. Oltmans, 1998: Upper tropospheric relative humidity observations and implications for cirrus ice nucleation. – Geophys. Res. Lett. **25**, 1343–1346.

Immler, F., J. Dykema, T. Gardiner, P.T.D.N. Whiteman, H. Vömel, 2010: Reference quality upper-air measurements: guidance for developing GRUAN data products. – Atmos. Meas. Tech. **3**, 1217–1231.

Irvine, E., K. Shine, 2015: Ice supersaturation and the potential for contrail formation in a changing climate. – Earth Syst. Dynam. **6**, 555–568, DOI: 10.5194/esd-6-555-2015.

Jackson, D., J. Bates, 2001: Upper tropospheric humidity algorithm assessment. – JGR **106**, 32259–32270.

Kempter, S., 2016: Analyse von dicken eisübersättigten Schichten unter Verwendung von HIRS-Daten. – Bachelor's thesis, Universität Augsburg, Institut für Geographie.

Koop, T., B. Luo, A. Tsias, T. Peter, 2000: Water activity as the determinant for homogeneous ice nucleation in aqueous solutions. – Nature **406**, 611–614.

Krämer, M., C. Rolf, A. Luebke, A. Afchine, N. Spelten, A. Costa, J. Meyer, M. Zöger, J. Smith, R. Herman, B. Buchholz, V. Ebert, D. Baumgardner, S. Borrmann, M. Klingebiel, L. Avallone, 2016: A microphysics guide to cirrus clouds part 1: Cirrus types. – Atmos. Chem. Phys. **16**, 3463–3483, DOI: 10.5194/acp-16-3463-2016.

Limpert, E., W. Stahel, M. Abbt, 2001: Log-normal distributions across the sciences: Keys and clues. – BioScience **51**, 341–352.

Marenco, A., V. Thouret, P. Nedelec, H. Smit, M. Helten, D. Kley, F. Karcher, P. Simon, K. Law, J. Pyle, G. Poschmann, R.V. Wrede, C. Hume, T. Cook, 1998: Measurement of Ozone and water vapor by Airbus In-service airCraft: The MOZAIC airborne program, an overview. – J. Geophys. Res. **103**, 25631–25642.

Mech, M., L.L. Kliesch, A. Anhäuser, T. Rose, P. Kallias, S. Crewell, 2019: Microwave radar/radiometer for arctic clouds (MIRAC): first insights from the ACLOUD campaign. – Atmos. Meas. Tech. **12**, 5019–5037, DOI: 10.5194/amt-12-5019-2019.

Neis, P., 2017: Water vapour in the UTLS – climatologies and transport. – Ph.D. thesis, Johannes Gutenberg-Universität Mainz, Germany.

Ovarlez, J., J.F. Gayet, K. Gierens, J. Ström, H. Ovarlez, F. Auriol, R. Busen, U. Schumann, 2002: Water vapour measurements inside cirrus clouds in northern and southern hemispheres during INCA. – Geophys. Res. Lett. **29**, 1813, DOI: 10.1029/2001GL014440.

Petzold, A., V. Thouret, C. Gerbig, A. Zahn, C. Brenninkmeijer, M. Gallagher, M. Hermann, M. Pontaud, H. Ziereis, D. Boulanger, J. Marshall, P. Nedelec, H. Smit, U. Friess, J.M. Flaud, A. Wahner, J.P. Cammas, A. Volz-Thomas, 2015: Global-scale atmosphere monitoring by in-service aircraft – current achievements and future prospects of the European research infrastructure IAGOS. – Tellus B **67**, DOI: 10.3402/tellusb.v67.28452.

Petzold, A., P. Neis, M. Rütimann, S. Rohs, F. Berkes, H. Smit, M. Krämer, N. Spelten, P. Spichtinger, P. Nedelec, A. Wahner, 2019: Vertical distribution, seasonality and tropospherecity of ice-supersaturated air masses in the nothern mid-latitudes from regular in-situ observations by passenger aircraft. – Atmos. Chem. Phys. Discuss. **19**, 1–29, DOI: 10.5194/acp-2019-735.

Rädel, G., K. Shine, 2007: Evaluation of the use of radiosonde humidity data to predict the occurrence of persistent contrails. – Quart. J. Roy. Met. Soc. **133**, 1413–1423.

Scarlat, R., C. Melsheimer, G. Heygster, 2018: Retrieval of total water vapour in the arctic using microwave humidity sounders. – Atmos. Meas. Tech. **11**, 2067–2084, DOI: 10.5194/amt-11-2067-2018.

Sherwood, S., W. Ingram, Y. Tsushima, M. Satoh, M. Roberts, P. Vidale, P. O'Gorman, 2010: Relative humidity changes in a warmer climate. – J. Geophys. Res. **115**, D09104, DOI: 10.1029/2009JD012585.

Sioris, C., J. Zou, D. Plummer, C. Boone, C. McElroy, P. Sheese, O. Moeini, P. Bernath, 2016: Upper tropospheric water vapour variability at high latitudes – part 1: Influence of the annular modes. – Atmos. Chem. Phys. **16**, 3265–3278, DOI: 10.5194/acp-16-3265-2016.

Spichtinger, P., K. Gierens, W. Read, 2003a: The global distribution of ice-supersaturated regions as seen by the Microwave Limb Sounder. – Quart. J. Roy. Met. Soc. **129**, 3391–3410.

Spichtinger, P., K. Gierens, U. Leiterer, H. Dier, 2003b: Ice supersaturation in the tropopause region over Lindenberg, Germany. – Meteorol. Z. **12**, 143–156.

Spichtinger, P., K. Gierens, H. Smit, J. Ovarlez, J.F. Gayet, 2004: On the distribution of relative humidity in cirrus clouds. – Atmos. Chem. Phys. **4**, 639–647.

Thompson, D., J. Wallace, 2000: Annular modes in the extratropical circulation. part I: Month-to-month variability. – J. Climate **13**, 1000–1016.

Treffeisen, R., R. Krejci, J. Ström, A. Engvall, A. Herber, L. Thomason, 2007: Humidity observations in the arctic troposphere over Ny-Ålesund, Svalbard based on 15 years of radiosonde data. – Atmos. Chem. Phys. **7**, 2721–2732.

Weaver, D., K. Strong, M. Schneider, P. Rowe, C. Sioris, K. Walker, Z. Mariani, T. Uttal, C. McElroy, H. Vömel, A. Spassiani, J. Drummond, 2017: Intercomparison of atmospheric water vapour measurements at a Canadian high arctic site. – Atmos. Meas. Tech. **10**, 2851–2880, DOI: 10.5194/amt-10-2851-2017.

Weaver, D., K. Strong, K. Walker, C. Sioris, M. Schneider, C. McElroy, H. Vömel, M. Sommer, K. Weigel, A. Rozanov, J. Burrows, W. Read, E. Fishbein, G. Stiller, 2019: Comparison of ground-based and satellite measurements of water vapour vertical profiles over Ellesmere island, Nunavut. – Atmos. Meas. Tech. **12**, 4039–4063, DOI: 10.5194/amt-12-4039-2019.

Wegener, A., 1914: Meteorologische Terminbeobachtungen am Danmarks-Havn. – In: Meddelelser om Grønland, Vol. XLII: Danmark-Ekspeditionen til Grønlands Nordøstkyst 1906–1908, Vol. II, Kommissionen for ledelsen af de geologiske og geografiske undersøgelser i Grønland, 125–356.

Wright, J., A. Sobel, J. Galewsky, 2010: Diagnosis of zonal mean relative humidity changes in a warmer climate. – J. Climate **23**, 4556–4569, DOI: 10.1175/2010JCLI3488.1.